Molecular Dynamics Study of the Ionic Liquid 1-*n*-Butyl-3-methylimidazolium Hexafluorophosphate

Timothy I. Morrow and Edward J. Maginn*

Department of Chemical Engineering, University of Notre Dame, Notre Dame, Indiana 46556

Received: August 6, 2002; In Final Form: October 4, 2002

We report the results of a molecular dynamics study of the ionic liquid 1-*n*-butyl-3-methylimidazolium hexafluorophosphate [bmim][PF_6], a widely studied ionic liquid. An all-atom force field is developed using a combination of density functional theory calculations and CHARMM 22 parameter values. Molecular dynamics simulations are carried out in the isothermal−isobaric ensemble at three different temperatures. Quantities computed include infrared frequencies, molar volumes, volume expansivities, isothermal compressibililties, self-diffusivities, cation−anion exchange rates, rotational dynamics, and radial distribution functions. Computed thermodynamic properties are in good agreement with available experimental values.

1. Introduction

The term ionic liquid (IL) has been coined in recent years to describe a class of organic salts that are liquid in their pure state at or near room temperature.[1] Some of the more widely studied ILs consist of a heterocyclic cation based on a substituted pyridine or imidazole and an inorganic anion. Early studies focused on compounds with the $[AlCl_4]^-$ anion, but these liquids proved to be unstable in air. This problem was overcome[2] through the use of alternative anions such as $[BF_4]^-$, $[NO_3]^-$, $[CH_3COO]^-$, and $[PF_6]^-$. These stable ILs have attracted a great deal of interest because of their potential as nonvolatile (and hence potentially environmentally benign) solvents.[3] They also show potential for a range of other applications including separations, industrial cleaning, fuel cells, lubricants, and heat transfer fluids.[4]

Compared to conventional organic solvents, relatively little is known about the thermodynamic and transport properties of ILs and how these properties relate to chemical constitution and structure. In addition to experimental efforts directed at this problem, a few theoretical studies have been reported in which quantum chemical[5] and classical condensed phase simulations[6−8] were used to examine structural and thermophysical properties of water-stable ILs. Other theoretical studies have focused on chloroaluminate-based ILs.[9−11]

The present work reports results of single molecule quantum chemical calculations and condensed phase classical molecular dynamics (MD) simulations on the ionic liquid 1-*n*-butyl-3-methylimidazolium hexafluorophosphate, which will be abbreviated as [bmim][PF_6]. Figure 1 shows the optimized geometry of a single [bmim][PF_6] molecule in the gas phase, obtained from a density functional theory calculation (see below). The atom labels shown in this figure will be referred to throughout the work.

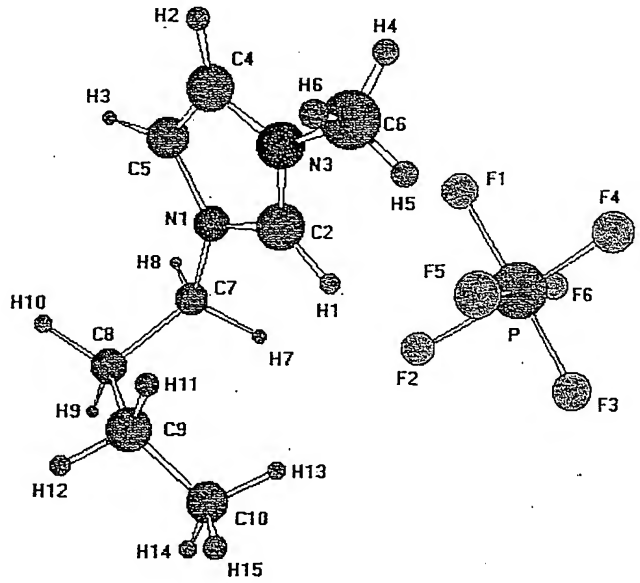

Figure 1. Geometry optimized structure of [bmim][PF_6] with atom labels noted.

2. Force Field

The extent to which a classical molecular simulation accurately predicts thermophysical properties depends on the quality of the force field used to model the interactions in the fluid. In this work, we have used a standard molecular mechanics force field,[12] with functional form

$$V_{tot} = \sum_{bonds} k_b(r - r_0)^2 + \sum_{angles} k_\theta(\theta - \theta_0)^2 + \sum_{dihedrals} k_\chi[1 + \cos(n\chi - \delta)] + \sum_{improper} k_\psi(\psi - \psi_0)^2 + \sum_{i=1}^{N-1}\sum_{j>i}^{N}\left\{\epsilon_{ij}\left[\left(\frac{r_{min,ij}}{r_{ij}}\right)^{12} - \left(\frac{r_{min,ij}}{r_{ij}}\right)^{6}\right] + \frac{q_i q_j}{r_{ij}}\right\} \quad (1)$$

where V_{tot} is the total energy of the system, harmonic potentials govern bond length, bond angle, and improper angle motion about nominal values r_o, θ_0, and ψ_0 and dihedral angles are modeled using a standard cosine series. The Lennard-Jones parameters for unlike atoms, ϵ_{ij} and $r_{min,ij}$, are obtained using the Lorentz−Berthelot combining rule. Coulombic interactions are modeled using fixed partial charges on each atom center.

* To whom correspondence should be addressed. E-mail: ed@nd.edu.

10.1021/jp0267003 CCC: $22.00
Published on Web 11/16/2002

TABLE 1: Partial Atomic Charges and Lennard-Jones Parameters Used in This Work

atom	q_i (e)	$r_{min,i}$ (Å)	ϵ_i (kJ mol^{-1})	atom	q_i (e)	$r_{min,i}$ (Å)	ϵ_i (kJ mol^{-1})
C_4	−0.141	3.600	0.209	H_9	0.055	2.680	0.117
C_5	−0.217	3.600	0.209	H_{10}	0.001	2.680	0.117
N_1	0.111	3.700	0.837	C_9	0.256	4.020	0.234
C_2	0.056	3.600	0.209	H_{11}	−0.029	2.680	0.117
N_3	0.133	3.700	0.837	H_{12}	−0.099	2.680	0.117
H_2	0.181	2.936	0.033	C_{10}	−0.209	4.080	0.326
H_3	0.207	2.936	0.033	H_{13}	0.051	2.680	0.100
H_1	0.177	1.800	0.192	H_{14}	0.040	2.680	0.100
C_6	−0.157	4.550	0.084	H_{15}	0.075	2.680	0.100
H_4	0.125	2.640	0.092	P_1	1.458	4.30	2.448
H_5	0.073	2.640	0.092	F_1	−0.421	3.400	0.377
H_6	0.142	2.640	0.092	F_2	−0.426	3.400	0.377
C_7	0.095	4.550	0.084	F_3	−0.368	3.400	0.377
H_7	0.055	2.680	0.092	F_4	−0.368	3.400	0.377
H_8	0.045	2.680	0.092	F_5	−0.364	3.400	0.377
C_8	−0.122	4.020	0.234	F_6	−0.414	3.400	0.377

With the exception of r_0, θ_0, and ψ_0 all cation intramolecular and Lennard-Jones parameters in eq 1 were taken directly from the CHARMM 22 force field[13] and used without modification. For the anion, bond length and bond angle parameters were derived from ab initio calculations, as described below. CHARMM 22 Lennard-Jones parameters were used for phosphorus and fluorine.

The minimum-energy geometry of the [bmim] cation and the [PF_6] anion was determined by performing ab initio geometry optimizations on the isolated cation and anion at the B3LYP/6-311+G* level of theory using Gaussian 98.[14] Cation and anion charges were set at +1 and −1, respectively. The resulting minimized structure was used to set r_0, θ_0, and ψ_0. Geometry optimization was also carried out on the [bmim][PF_6] pair at the same level of theory. The anion was initially located well away (over 10 Å) from the cation and facing the imidazolium C_2-carbon side. The minimum energy structure agrees very well with the results of Meng et al.[5] Partial atomic charges were derived from this geometry using the CHELPG[15] method. A listing of all force field parameters is given in Tables 1 and 2. We note that the pair calculations yielded total charges on the cation and anion of +0.904 and −0.904, respectively. In addition, the anion is slightly polarized (i.e., the charges on the fluorine atoms are not symmetric). For most of the simulations, we used these partial charges as a simple approximation of the induced polarization of the ions that occur in the liquid. This turned out not to be essential, given that the anion exhibited no preferential orientation relative to the nearest cation, as determined by monitoring the fraction of the time a given fluorine atom was closest to the C_2 carbon of the cation. We also performed simulations on an anion with symmetric charges totaling −0.904 and found essentially no difference in the computed properties.

The force constants k_b and k_θ for the anion were determined by performing a vibrational analysis on the geometry-optimized pair within Gaussian 98. The normal modes corresponding to

TABLE 2: Bond, Angle, Dihedral, and Improper Force Constants

force	force constant		force	force constant	
bonds	k_b (kJ mol^{-1} Å^{-2})	r_0 (Å)	bonds	k_b (kJ mol^{-1} Å^{-2})	r_0 (Å)
C_6–N_3	220.0	1.470	C_7–$H_{7,8}$		1.091
C_7–N_1	220.0	1.483	$C_{8,9}$–$H_{9,10,11,12}$		1.096
$C_{5,4}$–$N_{1,3}$	400.0	1.382	C_{10}–$H_{13,14,15}$		1.093
C_2–$N_{1,3}$	400.0	1.337	C_7–C_8	200.0	1.530
C_4–C_5	410.0	1.361	C_8–C_9	222.5	1.534
C_2–H_1		1.078	C_9–C_{10}	222.5	1.530
$C_{4,5}$–$H_{2,3}$		1.078	P–F	260.3	1.646
C_6–$H_{4,5,6}$		1.089			

angles	k_θ (kJ mol^{-1} rad^{-2})	θ_0 (deg)	angles	k_θ (kJ mol^{-1} rad^{-2})	θ_0 (deg)
C_8–C_7–N_1	140.0	112.6	$H_{4,5,6}$–C_6–H	35.5	109.3
$C_{5,4}$–$N_{1,3}$–C_2	130.0	125.9	$H_{7,8}$–C_7–H	35.5	107.2
$H_{4,5,6}$–C_6–N_3	30.0	109.6	$H_{7,8}$–C_7–C_8	33.4	111.5
H_1–C_2–$N_{1,3}$	30.0	106.8	$H_{9,10}$–C_8–C_7	33.4	109.5
N_1–C_5–C_4	130.0	107.2	$C_{7,8}$–$C_{8,9}$–$C_{9,10}$	58.4	111.6
N_1–C_2–N_3	130.0	109.1	H–$C_{8,9}$–H	34.5	106.4
$N_{1,3}$–C_2–H_1	25.0	125.5	$C_{8,9}$–$C_{9,10}$–H	34.6	109.7
$H_{2,3}$–$C_{4,5}$–C	25.0	130.8	$H_{13,14,15}$–C_{10}–H	35.5	107.6
N_3–C_4–H_2	25.0	122.1	F–P–F	194.1	90.0

dihedral	k_χ (kJ mol^{-1})	n	δ (deg)	dihedral	k_χ (kJ mol^{-1})	n	δ (deg)
C_2–N_3–C_4–C_5	14.0	2	180	H_2–C_4–N_3–C_2	3.0	2	180
N_1–C_5–C_4–N_3	14.0	2	180	$N_{1,3}$–$C_{5,4}$–$C_{4,5}$–$H_{2,3}$	3.0	2	180
N_1–C_2–N_3–C_4	14.0	2	180	$N_{1,3}$–C_2–$N_{3,1}$–$C_{6,7}$	0.0	2	180
H_1–C_2–$N_{1,3}$–$C_{5,4}$	3.0	2	180	H_1–C_2–$N_{3,1}$–$C_{6,7}$	0.0	2	180
H_2–C_4–C_5–H_3	2.0	2	180	$H_{2,3}$–$C_{4,5}$–$N_{3,1}$–$C_{6,7}$	0.0	2	180
$C_{4,5}$–$C_{5,4}$–$N_{1,3}$–$C_{7,6}$	0.0	1	0	C_2–$N_{1,3}$–$C_{7,6}$–H	0.195	2	180

dihedral	k_χ (kJ mol^{-1})	n	δ (deg)	dihedral	k_χ (kJ mol^{-1})	n	δ (deg)
$C_{4,5}$–$N_{3,1}$–$C_{6,7}$–H	0.0	3	0	N_1–C_7–C_8–$H_{9,10}$	0.0	3	0
C_2–$N_{3,1}$–C_7–C_8	0.1	3	180	C_7–C_8–C_9–C_{10}	0.15	1	0
C_5–N_1–C_7–C_8	0.2	4	0	$H_{7,8}$–C_7–C_8–$H_{9,10}$	0.195	3	0
N_1–C_7–C_8–C_9	0.0	3	0	H,C–C_8–C_9–H,C	0.195	3	0
H,C–C_9–C_{10}–H	0.16	3	0				

improper	k_ψ (kJ mol^{-1} rad^{-2})	ψ_0 (deg)	improper	k_ψ (kJ mol^{-1} rad^{-2})	ψ_0 (deg)
H_1–N_1–N_3–C_2	0.50	0	$H_{2,3}$–$N_{3,1}$–$C_{4,5}$–C	0.5	0
$N_{1,3}$–$C_{4,5}$–C_2–$C_{6,7}$	0.6	0			

the stretching of a P−F bond and the bending of an F−P−F bond were identified using Gaussview, a graphical interface for the Gaussian program, and the computed vibrational frequencies were used to calculate the corresponding harmonic force constants. The geometry and force constants for the cation and anion are summarized in Table 2. In a similar manner, vibrational assignments for the major fundamental modes of the pair were made and compared against experimental infrared spectroscopy measurements,[16,17] as described in the Results section.

3. Simulation Details

Molecular dynamics simulations of 300 [bmim] cations and 300 [PF_6] anions were performed with the program NAMD[18] version 2.4 in a cubic cell with standard periodic boundary conditions. The simulations were carried out in the isothermal−isobaric (NPT) ensemble using a Nosé-Hoover barostat to maintain a pressure of 0.98 atm. The temperature was controlled via Langevin dynamics with a damping factor of 5 ps^{-1}. Initial configurations were generated by randomly inserting cation−anion pairs into the simulation box. To prevent overlap, an insertion was rejected if any of the newly inserted atoms were within 0.75 Å of any existing atoms. The initial configurations were relaxed using a conjugant−gradient energy minimization scheme. For most of the simulations, the initial cell volume was chosen to match the experimental density of the state point of interest. All of the C−H bonds were held rigid using the SHAKE[19] algorithm. The r-RESPA[20] multiple time-stepping algorithm was used with a time step of 2 fs for bonded and van der Waals interactions and 4 fs for electrostatic interactions. The dispersion interactions were cut off beyond 20.0 Å. A switching function, initiated at a distance of 18.5 Å, was used to bring the dispersion interactions smoothly to zero at the cutoff distance. Long-range electrostatic interactions were computed using the particle mesh Ewald method.[21,22]

Prior to conducting a production run, the total energy and cell volumes were monitored until steady-state was reached. Equilibration times varied from 700 to 1000 ps, after which production runs lasting 4 ns were started. The thermodynamic properties of the system (total energy, pressure, temperature, kinetic, and potential energy contributions) were saved to disk every 100 time steps, and the atomic coordinates were saved to disk every 400 time steps. All classical simulations of [bmim][PF_6] were conducted at atmospheric pressure (0.98 bar) and at the temperatures 298, 323, and 343 K.

The program NAMD was chosen primarily because it is a parallel MD program that scales remarkably well with the number of processors. Simulations were run on a cluster of eight Dell Precision 530 computers running Linux. Each node contains two Intel Xeon processors operating at 1.7 GHz. A 4 ns simulation of 300 IL molecules (9600 atoms) took approximately 300 h (12.5 days) to complete.

4. Results and Discussion

Figure 2 shows the experimental[16,17] and computed IR spectra for [bmim][PF_6]. The relevant peaks in the spectra are labeled I−V. The computed frequencies of the major vibrational modes agree well with experiment. Using Gaussview, peak I was visually identified as the out-of-plane bending of the $C_2-N_1-C_5$ angle in the imidazolium ring, peak II is the F−P−F bending motion, peak III is the in-plane bending of H−C−N angles in the imidazolium ring, peak IV is the vibrational motion of several atoms in the imidazolium ring, and the peaks in region V are the stretching of C−H bonds. The computed frequency

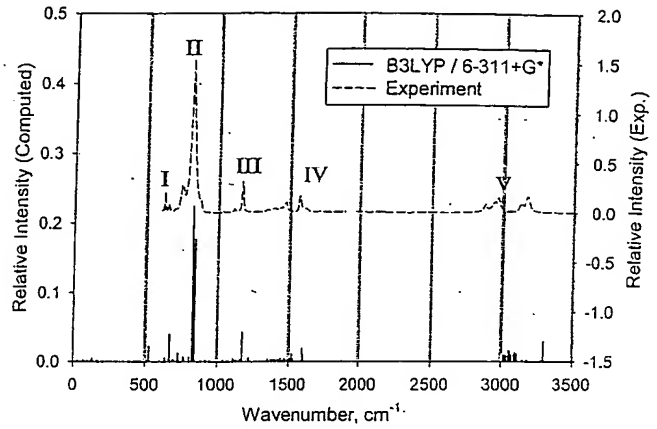

Figure 2. Comparison of computed and experimental[16] IR spectra for [bmim][PF_6].

TABLE 3: Comparison of Predicted and Experimental IR Spectral Data

assignment	pred. freq. (cm^{-1})	expt.[16] freq. (cm^{-1})
$C_2-N_1-C_5$ bend	669.9	622.9
F−P−F bend	827.5	815.8
imidazole H−C−C & H−C−N bend	1179.5	1167.7
imidazole ring bends	1600.9	1574.6
aliphatic C−H str.	3049.2	2939.1
aliphatic C−H str.	3092.9	2966.1
imidazole C−H str.	3294.8	3124.2
imidazole C−H str.	3299.3	3170.5

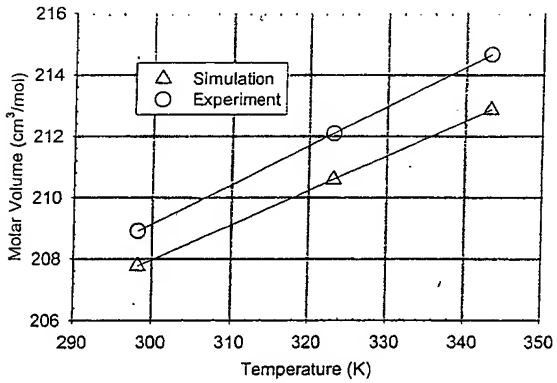

Figure 3. Comparison of predicted and experimental molar volumes of [bmim][PF_6] at 0.98 bar. Lines are linear fits to the data.

for peak I occurs at 50 cm^{-1} less than the experimental value. The agreement between computed and experimental frequencies for peaks II−IV is excellent. Peaks II and III occur at 15 cm^{-1} less than the experimental values, and peak IV occurs at 26 cm^{-1} less than the experimental value. The computed frequencies above 2800 cm^{-1} (region V) are overestimated, with errors larger than 100 cm^{-1} (see Table 3). The large errors in the predicted C−H stretching frequencies are likely due to anharmonicity effects.[23]

4.1. Molar Volume. Figure 3 shows the experimental[24] and computed molar volumes as a function of temperature at atmospheric pressure. Results are also given in Table 4. At all temperatures, the predicted molar volumes are lower than the experimental molar volumes by less than 1%. This level of agreement is excellent considering that the calculations are purely predictive; none of the force field parameters have been adjusted to match experimental data. Table 5 gives the breakdown of the potential energy into electrostatic, van der Waals, intramolecular, and kinetic energies. The average

TABLE 4: Comparison of Predicted and Experimental Molar Volumes, Volume Expansivities, and Isothermal Compressibilities at 0.98 Bar

	V (cm^3 mol^{-1})		$\alpha_P \times 10^4$ (K^{-1})		$\kappa_T \times 10^6$ (bar^{-1})	
temp (K)	sim	exp[24]	sim	exp[24]	sim	exp[24]
298.2	207.8	208.9	5.49	6.11	36.83	41.95
323.2	210.6	212.1	5.42	6.02	32.86	49.35
343.2	212.9	214.7	5.36	5.95	39.20	N/A

TABLE 5: Comparison of the Contribution of Various Terms to the System Total Energy

temp (K)	elect. (kJ/mol)	LJ (kJ/mol)	kinetic (kJ/mol)	intra. (kJ/mol)
298.2	−256.72	−89.22	100.50	89.56
323.2	−256.21	−87.19	108.92	96.74
343.2	−255.07	−85.51	116.78	102.4

electrostatic contribution to the potential energy at 298 K is −256.7 kJ/mol, which is twice as large as the van der Waals interactions and is 46 kJ/mol larger than the value reported for [emim][$AlCl_4$].[9] The total intramolecular potential energy, calculated by summing the bond, angle, dihedral, and improper angle energies, is 89.6 kJ/mol. This suggests that properties are most sensitive to the electrostatic portion of the force field.

4.2. Volume Expansivity (α_P). The volume expansivity quantifies the extent to which the volume of a fluid changes with temperature at constant pressure, and is defined as

$$\alpha_P = \frac{1}{V}\left(\frac{\partial V}{\partial T}\right)_P \tag{2}$$

The volume expansivity can be computed by running a series of simulations at the same pressure but different temperatures. Because the change of volume with temperature is approximately linear, α_P can be calculated using eq 2 by fitting a straight line to the simulated molar volume data. Table 4 lists the volume expansivities computed using this approach compared with the experimental results.[24] In all cases, the simulations predict expansivities that are lower than the experimental values by about 0.6 K^{-1}. It is observed that the predicted expansivities decrease slightly with increasing temperature, in good agreement with the experiments.

4.3. Isothermal Compressibility (κ_T). The isothermal compressibility quantifies the extent to which the volume of a fluid changes with pressure at constant temperature, and is defined as

$$\kappa_T = -\frac{1}{V}\left(\frac{\partial V}{\partial P}\right)_T \tag{3}$$

In this work, the isothermal compressibility was calculated using the following fluctuation formula[25]

$$\kappa_T = \frac{\langle \delta V^2 \rangle_{NPT}}{\langle V \rangle_{NPT} kT} \tag{4}$$

Table 4 lists the computed isothermal compressibilities compared with experimental values.[24] The computed isothermal compressibilities are consistently lower than the experimental values by 12−33%. There is still reasonably good agreement with experiment, however, especially considering the well-known difficulty in computing pressures from an atomistic simulation, as well as the inherent inaccuracy involved in computing derivative quantities using a fluctuation formula of the type in eq 4. The overall good agreement between the calculated and experimental PVT properties for this fluid indicates that the force field does a reasonable job of describing the liquid state of [bmim][PF_6]. The force field was therefore used to compute other thermodynamic, structural, and dynamic properties for which experimental data do not yet exist.

TABLE 6: Self-Diffusion Coefficients and Cohesive Energy Density of [bmim][PF_6] versus Temperature

temp (K)	$D_{[bmim]} \times 10^{-12}$ (m^2 s^{-1})	$D_{[PF_6]} \times 10^{-12}$ (m^2 s^{-1})	c (J cm^{-3})
298.2	9.70 ± 4.1	8.82 ± 4.2	761
323.2	15.4 ± 5.8	11.1 ± 5.6	738
343.2	12.1 ± 7.3	10.6 ± 7.6	727

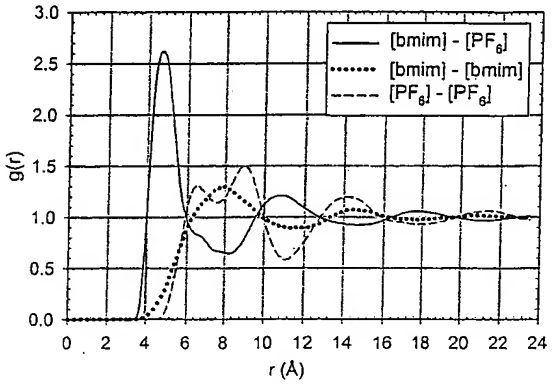

Figure 4. Center of mass radial distribution functions of [bmim][PF_6] at 298 K and 0.98 bar.

4.4. Cohesive Energy Density. The cohesive energy density of a liquid is defined as[26]

$$c = \frac{\Delta U^{vap}}{V^L} \tag{5}$$

where ΔU^{vap} is the change in internal energy of the liquid upon isothermal vaporization into the ideal gas state and V^L is the molar volume of the liquid. To calculate the cohesive energy density, the average internal energy and molar volume of the liquid were obtained from the liquid simulation, and the average internal energy of the ideal gas was obtained by simulating a single [bmim][PF_6] ion pair at the same temperature as the liquid but at zero pressure (i.e., no periodic boundary conditions). The cohesive energy density of [bmim][PF_6] versus temperature is given in Table 6. At 298 K, the cohesive energy density is 761 J cm^{-3}. In contrast, the cohesive energy densities of the heavy hydrocarbons hexadecane and naphthalene are 268 and 410 J cm^{-3}, respectively.[27] The extremely high cohesive energy density of [bmim][PF_6] stems mainly from electrostatic interactions, and explains why these liquids have such low volatility.

4.5. Molecular Structure. To obtain a better understanding of the structure of this ionic liquid, various radial distribution functions (RDFs or $g(r)$) were computed at each of the statepoints. The center-of-mass RDFs for cation−cation, cation−anion, and anion−anion pairs at 298 K and 0.98 bar are shown in Figure 4. The RDFs at 323 and 343 K are qualitatively very similar and are not shown here. It is observed that the first solvation shell for cation−anion pairs forms at about 4.3 Å. The second and third cation−anion solvation shells occur at 10.6 and 17.6 Å, respectively. Given the long-range Coulombic interactions in this system, it is not surprising to see that weak ordering persists beyond 23 Å. The first peak in the cation−cation RDF occurs at 8 Å, and the anion−anion RDF shows two peaks at 6.5 and 9 Å. This split peak is the result of sequential ordering induced by the cation−anion pairs. The RDFs agree remarkably well with those of Shah et al.,[8] who used a simpler, united atom model for this liquid.

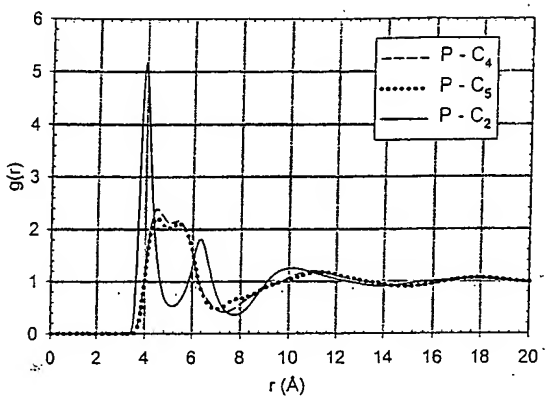

Figure 5. Atom–atom radial distribution functions for [bmim][PF6] at 298 K and 0.98 bar.

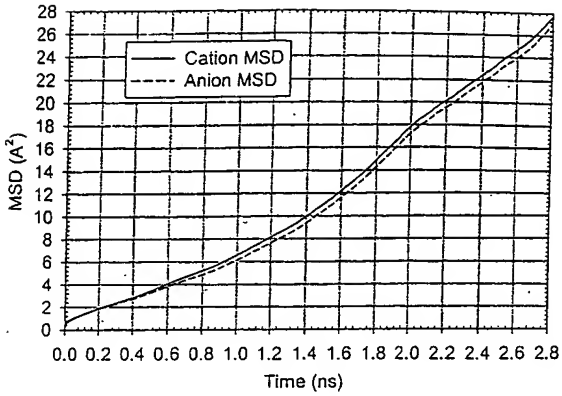

Figure 6. Center of mass mean square displacements of [bmim][PF6] at 298 K and 0.98 bar.

Further insight into the liquid structure can be gained by examining the site–site pair RDFs. RDFs for the phosphorus atom of the anion and different imidazolium carbon atoms of the cation are shown in Figure 5. It is observed that the anion prefers to associate with the C_2 carbon of the imidazolium ring. The C_2–H_1 atom pair constitutes the largest amount of positive charge on the cation, so it is not surprising that the anion interacts more strongly with this part of the cation. In addition, the locations of the first peaks in the RDFs of Figure 5 are consistent with the ab initio optimized geometry of the cation–anion pair shown in Figure 1.

The RDFs suggest that the individual ions in [bmim][PF6] tend to aggregate into well-defined ion clusters. By integrating $g(r)$ out to the location of the first minimum, the coordination number for the first solvation shell, N, can be calculated via the following equation

$$N = \int_0^{r_{shell}} \rho g(r) 4\pi r^2 \, dr \qquad (6)$$

where ρ is the bulk density and r_{shell} is the first minimum in $g(r)$. Using r_{shell} equal to 8.36 Å, the calculated coordination number for the cation–anion first solvation shell is 6.8, indicating that each ion is surrounded by a cage of nearly seven other counterions. Similarly, the cation–cation coordination number is 6.2, and the anion–anion coordination number is 6.1. Therefore, the total coordination number for the first solvation shell of an ion is nearly 13. Note, however, that the coordination numbers computed from eq 6 are sensitive to the choice of r_{shell}. For example, setting r_{shell} equal to 8.0 Å reduces the cation–anion, cation–cation, and anion–anion coordination numbers to 6.2, 5.0, and 4.9, respectively.

4.6. Diffusion. The coefficient of self-diffusion for a fluid or solid can be calculated using the Einstein relation[28]

$$D_{Self} = \frac{1}{6} \lim_{t \to \infty} \frac{d}{dt} \langle |r_i(t) - r_i(0)| \rangle \qquad (7)$$

where the quantity in braces is the ensemble-averaged mean square displacement (MSD) of the molecules and r_i is the vector coordinate of the center of mass of ion i. The mean square displacements of the cation and anion at 298 K and 0.98 bar are shown in Figure 6. The MSDs are linear up to roughly 1 ns, after which they show a slightly nonlinear increase up to about 1.8 ns, followed by a second linear regime. A block averaging technique[25] was used to obtain the MSDs, so the results are most reliable at short times. For this reason, the self-diffusion coefficients for the cation and anion were obtained by fitting the slope of the linear region from 200 to 1000 ps to a straight line and applying eq 7. Results are given in Table 6.

At 298 K and 0.98 bar, the predicted self-diffusion coefficients of the cation and anion are 9.70×10^{-12} and 8.82×10^{-12} m^2 s^{-1}, respectively. For comparison, the self-diffusion coefficient of water[29] at 298 K and 1 atm is 2.3×10^{-9} m^2 s^{-1}. This result is consistent with the fact that [bmim][PF6] has a much higher viscosity (450 cP)[30] than water. If one assumes that the Stokes–Einstein relation can be applied to this system, then the self-diffusion coefficients for the ionic liquid can be estimated from the relation.

$$D_{IL} = D_{H_2O} \frac{\eta_{H_2O}}{\eta_{IL}} \qquad (8)$$

where $D_{IL} = 1/2(D_{[bmim]} + D_{[PF_6]})$ and η is the viscosity. Using eq 8 and $\eta_{H_2O} = 0.9$ cP,[31] the estimated self-diffusion coefficient for the ionic liquid is 4.6×10^{-12} m^2 s^{-1}, which is fairly close to the computed value, especially considering the simplifying assumptions behind the Stokes–Einstein relation. The computed self-diffusion coefficients for [bmim] and [PF6] are roughly 10 times smaller than those reported by de Andrade et al.,[9] who computed self-diffusivities for 1-ethyl-3-methylimidazolim ([emim]) and [AlCl4] ions and are also 10 times smaller than the experimental result for [emim].[32] This is not surprising because the [emim] and [AlCl4] ions are smaller than the ions in this study and because the reported intermolecular potential energy[9] for [emim][AlCl4] is not as great as it is in this system. The computed self-diffusion coefficient for [PF6] is also seven times lower than that calculated by Hanke et al.[6] from a simulation of dimethylimidazolium ([dmim]) [PF6] at 400 K. Much of this difference could be due to the fact that the simulations of Hanke et al.[6] were at higher temperatures than the present work and because [dmim] is a smaller cation than [bmim]. We also note that the simulations in both ref 6 and 9 were over a much shorter time scale (100 ps) compared to the relatively long simulation times of this work.

The self-diffusion coefficients for [bmim] and [PF6] could not be determined reliably by fitting the mean square displacement data at times longer than 1 ns. This was due to inaccuracies in the data caused by insufficient sampling. These inaccuracies were apparent in the relatively large (but not systematic) anisotropy in the diagonal terms of the self-diffusivity tensor at times greater than 1 ns. Long-time anisotropy in a homogeneous system indicates that even longer simulations than those in this work are needed to accurately determine MSDs above 1 ns. One must therefore leave open the possibility that the actual self-diffusivity, which by definition is a long-time quantity, may differ from that which is computed over these relatively short time scales. Nevertheless, the values reported here appear to

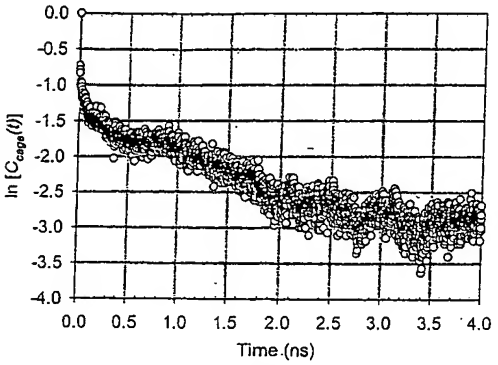

Figure 7. Time dependence of ln $[C_{cage}(t)]$ for [bmim][PF_6] at 298 K and 0.98 bar.

be reasonable estimates of the actual self-diffusivity, on the basis of the semiquantitative agreement with the results obtained from the Stokes–Einstein model. The validity of the self-diffusivity can also be tested through use of the following diffusion model.

Recalling that each ion is surrounded by a cage of other ions, we hypothesize that ion diffusion involves a two-step process. In the first step, neighboring ions are displaced enough to disrupt a cage and form a diffusion pathway. In the second step, an ion leaves its cage, moving to another neighboring cage site. To test this hypothesis, the characteristic time for the breaking of ion cages was determined through use of a cage correlation function.[33] The cage for a given ion is determined by the neighbor list for that ion, defined as

$$l_i \equiv \begin{pmatrix} f(r_{i1}) \\ \vdots \\ f(r_{iN}) \end{pmatrix} \tag{9}$$

where $f(r_{ij})$ is the Heaviside function

$$f(r_{ij}) = H(r_{cut} - r_{ij}) = \begin{cases} 1 & \text{if } r_{ij} \le r_{cut} \\ 0 & \text{otherwise} \end{cases} \tag{10}$$

and r_{cut} is a cutoff radius for the neighbor list. The cage correlation function is defined as

$$C_{cage}(t) \equiv \langle H(1 - n_i^{out}(0,t)) \rangle \tag{11}$$

where n_i^{out} is the number of ions that have left ion i's original neighbor list at time t and H is the Heaviside function. In computing the neighbor lists for all the ions, r_{cut} was set equal to the location of the first minimum of the cation/anion radial distribution function. Figure 7 shows ln $C_{cage}(t)$ for the system at 298 K. There is a rapid decay of $C_{cage}(t)$ at short times ($t <$ 0.5 ns), which is attributed to vibrational motion of ions near the boundary of a cage. After the period of initial rapid decay, $C_{cage}(t)$ plateaus and then decays exponentially after about 0.8–2.0 ns. It is interesting to note that 0.8 ns is about the same time in which a shift in the slopes of the MSDs is observed in Figure 6. By fitting an exponential function to the region from 0.8 to 2.0 ns, a time constant of 1.53 ns is obtained for the decay of the ion cages. This time constant is indicative of the average time needed for any particular ion to leave another ion's neighbor list.

To investigate the rate at which anions exit the ion cages, $C_{cage}(t)$ was computed by considering only the *anions* surrounding a given *cation*. A plot of ln $C_{cage}(t)$ at 298 K computed in this way is qualitatively similar to Figure 7 and is not shown here. The time constant obtained by fitting the intermediate region to an exponential is 3.46 ± 0.04 ns. Likewise, the rate at which cations exit the ion cages can be studied by computing ln $C_{cage}(t)$ by considering only the *cations* surrounding a given *anion*. The time constant computed for cation departure at 298 K is 3.25 ± 0.03 ns. It is not surprising to see that the time constant computed from Figure 7 is about half the time constants for cation and anion departures. This is because whenever a cation departs from an anion's neighbor list that cation simultaneously sees the anion depart from its own neighbor list. Thus, two cages decay whenever one ion moves out of another ion's cage.

The cage correlation results suggest that diffusion in ionic liquids can be modeled semiquantitatively as an activated hopping process. Each ion is assumed to reside on a three-dimensional lattice, with lattice spacings Δ given by the distance between peaks in $g(r)$. Ions execute a random walk between sites with a characteristic time τ, assumed to be equal to the time constant for cage decomposion. The self-diffusion coefficient for this model is simply[34]

$$D_{self} = \frac{\Delta^2}{6\tau} \tag{12}$$

To compute the self-diffusion coefficient for [bmim] using this model, we set Δ = 8 Å and τ = 3.25 ns. The resulting D_{self} for [bmim] is 3.28 × 10^{-11} m^2 s^{-1}. Using Δ = 8 Å and τ = 3.49 ns for [PF_6] gives a self-diffusivity of 3.08 × 10^{-11} m^2 s^{-1}. These results are roughly three times higher than the computed self-diffusivities and a factor of 10 greater than that estimated from the Stokes–Einstein model. It should be expected that this simple model over predicts the self-diffusivity, because it does not account for correlated hoping motion. In the real system, it is likely that an ion that leaves a cage will frequently return to its original location, thus decreasing the overall displacement. The simplified model does not account for this but rather assumes that ions successfully thermalize in a new cage after each hop. Nevertheless, this simple model appears to capture much of the dynamics responsible for diffusion in this system.

4.7. Test of Sampling. Figure 6 shows that at 298 K the average ion moves only about 2 Å per ns of simulation time. This sluggish dynamics raises a serious concern over the level of phase space sampling in the current simulations, as well as the suitability of molecular dynamics for these calculations. As a simple test to determine if the simulations were stuck in a local potential energy minimum, three additional 300 molecule simulations were conducted for [bmim][PF_6] at 298 K. Each simulation was started from a different initial configuration and at different initial densities. Figure 8 shows the molar volumes of each of these simulations versus time. All three independent simulations converged to the same molar volume as that found from the original simulation started near the experimental density within approximately 200 ps. This indicates that, although phase space sampling is still a concern for this system, it appears that the present calculations have been run long enough to properly sample the equilibrium state of the system.

4.8. Other Dynamic Properties. The rotational dynamics of the anion were investigated by computing the cosine of the average angle θ between the vector from the P atom to the F_1 atom of an anion at time zero and time t. The decorrelation of this angle with time gives insight into the rotational motion of the anion. The rotational time constant was obtained by fitting an exponential function to long-time decay of $\langle \cos \theta \rangle$. The

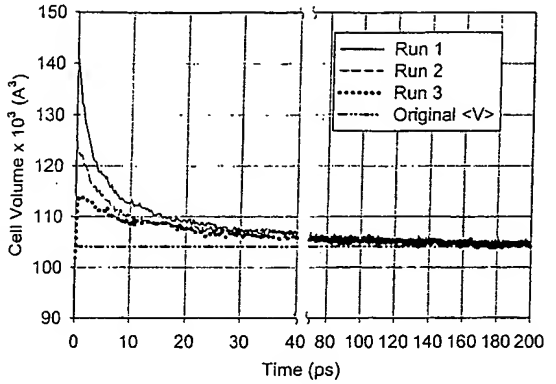

Figure 8. Plot of the cell volumes of three independent simulations of [bmim][PF_6] at 298 K and 0.98 bar. The horizontal dashed line is the average volume of the original simulation.

computed time constant for anion rotation at 298 K is approximately 28.8 ps. In a similar manner, the rotational dynamics of the cation were investigated using a vector normal to the imidazolium ring. As expected, the rotational time constant is much longer at approximately 4.3 ns. This huge separation of time scales is significant; although it appears that the translational motion of cations and anions is highly correlated and slow, their rotational motions occur over vastly different time scales.

5. Conclusions

Results of a molecular dynamics simulation of [bmim][PF_6] are reported. An all-atom force field for the ionic liquid is developed using a combination of ab initio calculations and CHARMM22 parameters. The agreement between the experimental and computed IR spectra is very good, and the vibrational motions associated with various peaks in the experimental spectrum are identified. The agreement between experimental and computed values of the volume expansivity and isothermal compressibility are good, and the agreement between molar volumes is excellent. The force field was not adjusted to match the experimental data. Discrepancies between the simulation and experiment may be due to the use of unoptimized potential parameters or the neglect of polarizability. Liquid structure is reported in the form of center-of-mass radial distribution functions for cation−cation, cation−anion, and anion−anion pairs, as well as site−site RDFs. It is observed that the anion tends to orient near the C_2 carbon of the cation. Self-diffusion coefficients for [bmim] and [PF_6] are computed from the slopes of the center-of-mass mean-square displacements of the cation and anion, respectively. The reported self-diffusivities are 2 orders of magnitude smaller than the self-diffusivity of water at room temperature. The mechanism for diffusion of the ions is investigated via the computation of cage correlation functions. A simple random walk diffusion model based on this time constant yields a self-diffusivity that is in fair agreement with the calculations, as does the Stokes−Einstein estimate based on scaling with the viscosity and diffusivity of water. Rotational dynamics of the cation and anion are investigated via the computation of a common order parameter. The rotational time constants are indicative of the very slow rotational dynamics of the [bmim] cation but the relatively fast rotational motion of the [PF_6] anion.

Acknowledgment. Support for this work was provided by the National Science Foundation under Grants CTS-9987627 and DMR-0079647. We gratefully acknowledge helpful discussions with Professor Joan F. Brennecke.

References and Notes

(1) Holbrey, J. D.; Seddon, K. R. *Clean Prod. Processes* **1999**, *1*, 223.
(2) Wilkes, J. S.; Zaworotko, M. J. *J. Chem. Soc., Chem. Commun.* **1992**, 965.
(3) Welton, T. *Chem. Rev.* **1999**, *99*, 2071.
(4) Brennecke, J. F.; Maginn, E. J. *AIChE J.* **2001**, *47*, 2384.
(5) Meng, Z.; Dölle, A.; Carper, W. R. *J. Mol. Struct. (THEOCHEM)* **2002**, *585*, 119.
(6) Hanke, C. G.; Price, S. L.; Lynden-Bell, R. M. *Mol. Phys.* **2001**, *99*, 801.
(7) Hanke, C. G.; Atamas, N. A.; Lynden-Bell, R. M. *Green Chem.* **2002**, *4*, 107.
(8) Shah, J. K.; Brennecke, J. F.; Maginn, E. J. *Green Chem.* **2002**, *4*, 112.
(9) de Andrade, J.; Böes, E. S.; Stassen, H. *J. Phys. Chem. B* **2002**, *106*, 3546.
(10) Takahashi, S.; Suzuya, K.; Kohara, S.; Koura, N.; Curtiss, L. A.; Saboungi, M. L. *Z. Phys. Chem.* **1999**, *209*, 209.
(11) Dymek, C. J., Jr.; Stewart, J. J. P. *Inorg. Chem.* **1989**, *28*, 1472.
(12) Leach, A. R. *Molecular Modelling: Principles and Applications*, 2nd ed.; Prentice Hall: New York, 2001.
(13) MacKerell, A. D.; Bashford, D.; Bellott, M.; Dunbrack, R. L.; Evanseck, J. D.; Field, M. J.; Fisher, S.; Gao, J.; Guo, H.; Ha, S.; Joseph-McCarthy, S.; Kuchnir, L.; Kuczera, K.; Lau, F. T. K.; Mattos, C.; Michnick, S.; Ngo, T.; Nguyen, D. T.; Prodhom, B.; Reiher, W. E., III.; Roux, B.; Schlenkrich, M.; Smith, J. C.; Stote, R.; Straub, J.; Watanabe, M.; Wiorkiewicz-Kuczera, J.; Yin, D.; Karplus, M. *J. Phys. Chem. B* **1998**, *102*, 3586.
(14) Frisch, M. J.; Trucks, G. W.; Schlegel, H. B.; Scuseria, G. E.; Robb, M. A.; Cheeseman, J. R.; Zakrzewski, V. G.; Montgomery, J. A., Jr.; Stratmann, R. E.; Burant, J. C.; Dapprich, S.; Millam, J. M.; Daniels, A. D.; Kudin, K. N.; Strain, M. C.; Farkas, O.; Tomasi, J.; Barone, V.; Cossi, M.; Cammi, R.; Mennucci, B.; Pomelli, C.; Adamo, C.; Clifford, S.; Ochterski, J.; Petersson, G. A.; Ayala, P. Y.; Cui, Q.; Morokuma, K.; Malick, D. K.; Rabuck, A. D.; Raghavachari, K.; Foresman, J. B.; Cioslowski, J.; Ortiz, J. V.; Stefanov, B. B.; Liu, G.; Liashenko, A.; Piskorz, P.; Komaromi, I.; Gomperts, R.; Martin, R. L.; Fox, D. J.; Keith, T.; Al-Laham, M. A.; Peng, C. Y.; Nanayakkara, A.; Gonzalez, C.; Challacombe, M.; Gill, P. M. W.; Johnson, B. G.; Chen, W.; Wong, M. W.; Andres, J. L.; Head-Gordon, M.; Replogle, E. S.; Pople, J. A. *Gaussian 98*, revision A.9; Gaussian, Inc.: Pittsburgh, PA, 1998.
(15) Brenneman, C. M.; Wiberg, K. B. *J. Comput. Chem.* **1990**, *11*, 361.
(16) Kazarian, S. IR data (personal communication).
(17) Suarez, P. A. Z.; Einloft, S.; Dullius, J. E. L.; de Souza, R. F.; DuPont, J. *J. Chim. Phys.* **1998**, *95*, 1626.
(18) Kale, L.; Skeel, R.; Bhandarkar, M.; Brunner, R.; Gursoy, A.; Krawetz, N.; Phillips, J.; Shinozaki, A.; Varadarajan, K.; Schulten, K. *J. Comput. Phys.* **1999**, *151*, 283.
(19) Ryckaert, J. P.; Ciccotti, G.; Berendsen, H. J. C. *J. Comput. Phys.* **1977**, *23*, 327.
(20) Tuckerman, M.; Berne, B. J.; Martyna, G. J. *J. Chem. Phys.* **1992**, *97*, 1990.
(21) Darden, T. A.; York, D. M.; Pedersen, L. G. *J. Chem. Phys.* **1993**, *98*, 10089.
(22) Essmann, U.; Perera, L.; Berkowitz, M. L.; Darden, T.; Lee, H.; Pedersen, L. G. *J. Chem. Phys.* **1995**, *103*, 8577.
(23) Koch, W.; Holthausen, M. C. *A Chemist's Guide to Density Functional Theory*, 2nd ed.; Wiley-VCH: New York, 2001.
(24) Gu, Z.; Brennecke, J. F. *J. Chem. Eng. Data* **2002**, *47*, 339.
(25) Allen, M. P.; Tildesley, D. J. *Computer Simulation of Liquids*; Clarendon Press: Oxford, U.K., 1987.
(26) Prausnitz, J. M.; Lichtenthaler, R. N.; de Azevedo, E. G. *Molecular Thermodynamics of Fluid Phase Equilibria*; Prentice Hall: New Jersey, 1999.
(27) Hildebrand, J. H.; Scott, R. L. *Regular Solutions*; Prentice Hall: New Jersey, 1962.
(28) Frenkel, D.; Smit, B. *Understanding Molecular Simulation*; Academic Press: New York, 1996.
(29) Hertz, H. G., Franks, F., Ed.; *Water, A comprehensive treatise*; Plenum Press: New York, 1973; Vol 3.
(30) Huddleston, J. G.; Visser, A. E.; Reichert, W. M.; Willauer, H. D.; Broker, G. A.; Rogers, R. D. *Green Chem.* **2001**, *3*, 156.
(31) Yaws, C. L.; Miller, J. W.; Shah, P. N.; Schorr, G. R.; Patel, P. M. *Chem. Eng.* **1976**, *83*, 153.
(32) Larive, C. K.; Lin, M.; Piersma, B.; Carper, W. R. *J. Phys. Chem.* **1995**, *99*, 12409.
(33) Rabani, E.; Gezelter, J. D.; Berne, B. J. *J. Chem. Phys.* **1997**, *107*, 6867.
(34) Reichl, L. E. *A Modern Course in Statistical Physics*; John Wiley & Sons: New York, 1998.